High Curie temperature for $La_{0.7}Sr_{0.3}MnO_3$ thin films deposited on CeO_2/YSZ-based buffered silicon substrates

P Perna[1,2,5], L Méchin[1], M P Chauvat[3], P Ruterana[3], Ch Simon[4] and U Scotti di Uccio[2]

[1] GREYC (UMR 6072)-CNRS-ENSICAEN, Universite Caen Basse-Normandie, 6 Boulevard Maréchal Juin, 14050 CAEN cedex, France
[2] CNR-INFM CRS Coherentia and Dipartimento Scienze Fisiche, Universita di Napoli Federico II, Complesso Universitario di Monte S Angelo, via Cinthia 80126 NAPOLI, Italy
[3] CIMAP (UMR 6252)-CNRS-CEA-ENSICAEN, Universite Caen Basse-Normandie, 6 Boulevard Maréchal Juin, 14050 CAEN cedex, France
[4] CRISMAT (UMR 6508)-CNRS-ENSICAEN, 6 Boulevard Maréchal Juin, 14050 CAEN cedex, France

E-mail: paolo.perna@imdea.org

Abstract

Two kinds of epitaxial structures were grown by standard pulsed laser deposition on (001) Si, namely $La_{0.7}Sr_{0.3}MnO_3/Bi_4Ti_3O_{12}/CeO_2$/YSZ/Si (BTO-based), and $La_{0.7}Sr_{0.3}MnO_3/SrTiO_3/CeO_2$ /YSZ/Si (STO-based) multilayers. The samples were investigated by means of x-ray diffraction, transmission electron microscopy, magnetic and transport measurements. The Curie temperature T_C of the BTO-based samples was found to be higher (360 K) than for the typical reference epitaxial LSMO film grown on (001) $SrTiO_3$ single crystal (345 K), due to high compressive in-plane strain. The STO-based samples show high structural quality, low roughness and high T_C (350 K), making them interesting candidates for use in innovative LSMO-based bolometers or spintronic devices operating at room temperature.

(Some figures in this article are in colour only in the electronic version)

1. Introduction

In the last decade, the scientific community dedicated large efforts to the integration of transition metal oxides in the conventional, silicon-based electronics and to the development of non-conventional devices based on such materials [1]. On one hand, the recent, tremendous fortune of finding *amorphous* HfO_2 as a high-*k* dielectric demonstrates the incredible potentialities for oxides in electronics. On the other hand, the *epitaxial* growth of oxides is still hindered by serious technological problems, mainly related to the reactivity of the Si surface with oxygen, the cation interdiffusion, the different thermal expansion and the lattice mismatch between oxide film and substrate. All these issues are inescapable if one is interested in the integration of perovskites, such as manganites, since the direct deposition on silicon results in polycrystalline films [2], while the best properties are always observed for highly epitaxial samples grown on single-crystal substrates such as $SrTiO_3$ (STO), $LaAlO_3$ (LAO) and $NdGaO_3$ (NGO) [3, 4].

A possibility for circumventing such problems is to introduce a buffer layer between Si and perovskite. One popular choice is yttria-stabilized zirconia (YSZ). YSZ presents the unique advantage that it activates the decomposition of the native SiO_2 at the interface with the substrate, with formation of ZrO_2 and desorption of SiO [5].

[5] Present address: IMDEA Nanociencia, Campus Universidad Autonóma de Madrid, 28049 Madrid, Spain.

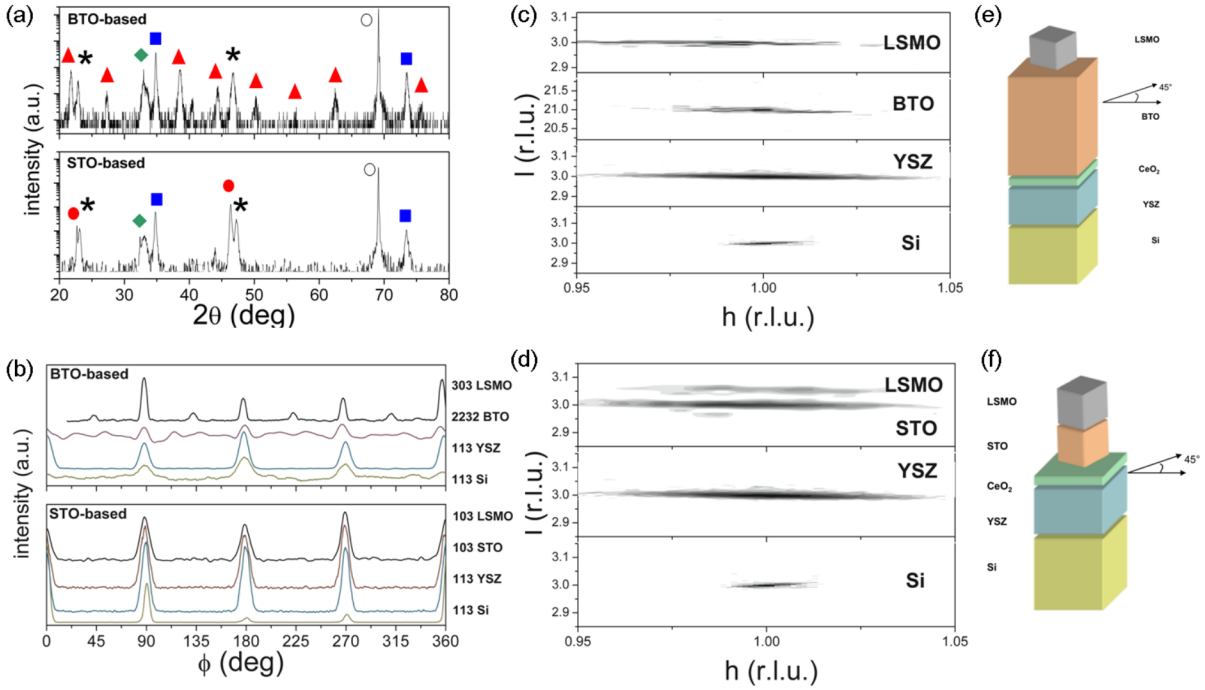

Figure 1. X-ray diffraction of the BTO- and STO-based LSMO (50 nm thick) samples: (a) 2θ–θ scans, where 'black star' means (00l) crystallographic reflections of LSMO, 'red triangle' of BTO, 'blue square' of YSZ, 'red circle' of STO, 'green diamond' of CeO_2 and 'open circle' of Si. (b) φ-scans. (c) RLMs around the asymmetric $(113)_{Si}$, $(113)_{YSZ}$, $(1\,1\,21)_{BTO}$ and $(103)_{LSMO}$ peaks of the BTO-based and (d) around the asymmetric $(113)_{Si}$, $(113)_{YSZ}$, $(103)_{STO}$ and $(103)_{LSMO}$ peaks of the STO-based sample. The sketches of the two multilayered structures are presented in (e) and (f).

Once the native amorphous SiO_2 layer is removed, YSZ grows epitaxially. These reactions are promoted in standard deposition systems with base pressure as high as $\approx 10^{-5}$ mbar, that is compatible with technological development [5, 6], while alternative processes may require extreme vacuum conditions (see, e.g., [7], reporting on the direct epitaxial growth of STO films on (001) Si by molecular beam epitaxy). However, the YSZ buffer is still insufficient for getting high quality manganite films. For example, Goh *et al* [8] demonstrated that $La_{0.7}Sr_{0.3}MnO_3$ (LSMO), when directly deposited on YSZ/Si, grows in a polycrystalline form. It is therefore necessary to implement more complex structures, by resorting to a multilayer of buffers (or templates). In [8], the authors report that a highly textured growth of LSMO can be obtained by resorting to a supplemental $YBa_2Cu_3O_{7-d}$ layer over YSZ. Fontcuberta *et al* [9] tried instead the buffer multilayers STO/CeO_2/YSZ/Si, STO/YSZ/Si and STO/TiN/YSZ/Si. The magnetic properties of LSMO were similar for the three buffers, with a Curie temperature T_C of about 350 K, but the transport properties revealed a relevant contribution of the intergrain resistance, with resistivity versus temperature $\rho(T)$ plots showing a far from ideal, broad maximum at $T_p \approx 200$ K. Finally, Kim *et al* [10, 11], showed that $La_{0.67}(Sr, Ca)_{0.33}MnO_3$ and $La_{0.75}Sr_{0.25}MnO_3$ films could be grown epitaxially on $Bi_4Ti_3O_{12}/CeO_2$/YSZ buffered (001) Si substrates due to a good lattice matching between materials.

In this paper, we present our work on multilayered buffers for the epitaxial growth of LSMO films on (001) Si using a standard deposition system. This is part of our research activity regarding the possible use of LSMO in infrared bolometers operating at room temperature [12], extending our widespread interest in application of LSMO to innovative electronic devices [13]. In bolometers, Si wafers are required to create suspended-bridge structures by resorting to standard micromachining procedures [14], aimed at reducing the thermal coupling with the substrate. Both applications demand LSMO films with high T_C and high structural quality.

2. Sample preparation and experimental details

A CeO_2/YSZ bilayer is first deposited on the Si substrate, with the function of a template for the subsequent growth of a buffer. We considered two different kinds of samples. The first series has the structure $La_{0.7}Sr_{0.3}MnO_3/Bi_4Ti_3O_{12}/CeO_2$/YSZ/Si (BTO-based case); the second has the structure $La_{0.7}Sr_{0.3}MnO_3/SrTiO_3/CeO_2$/YSZ/Si (STO-based case). Both structures are sketched in figures 1((e) and (f)). Their properties are compared to those of an epitaxial LSMO film directly grown on (001) $SrTiO_3$ single crystal, named the reference sample. All layers were deposited by pulsed laser deposition (PLD) in a chamber with 10^{-5} mbar base pressure at 700 °C. The KrF excimer laser (wavelength 248 nm) was operated at 3 Hz pulse rate. The energy density was 1–2 J cm^{-2} with 2×1 mm^2 spot size on the target that was at 50 mm from the substrate. The 10×10 mm^2 (001) Si substrates were clamped and radiantly heated from the back. No procedure aimed at removing the native oxide from the Si surface was adopted. During the YSZ deposition,

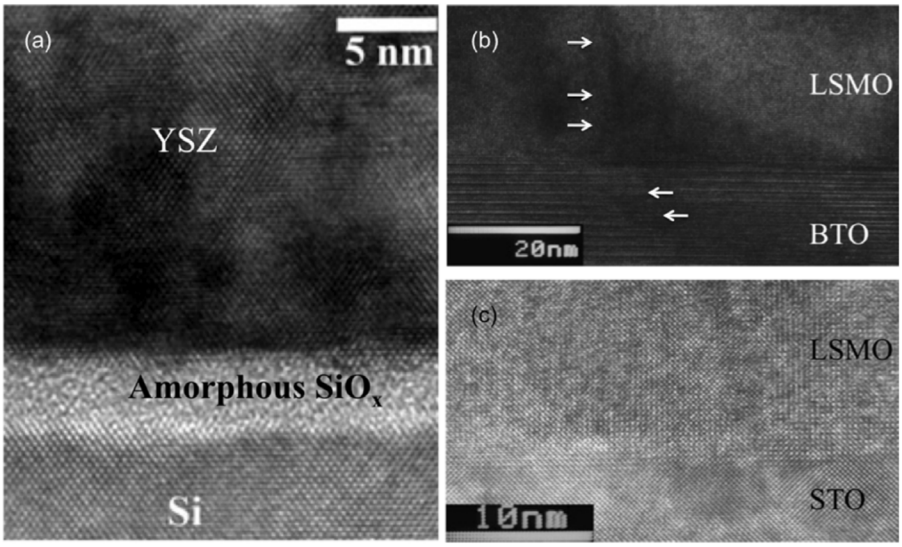

Figure 2. Transmission electron microscopy (TEM) cross-section photos of the (a) YSZ/Si, (b) LSMO/BTO and (c) LSMO/STO interfaces.

the substrate temperature was kept at 700 °C while the oxygen pressure was raised from 2×10^{-5} mbar, at the early stage of growth, to 10^{-4} mbar. The reducing atmosphere at the first stage of growth promotes the reaction $Zr + 2SiO_2 \rightarrow ZrO_2 + 2SiO$, enabling the subsequent epitaxial growth of (001) YSZ. The deposition temperature and oxygen pressure were fixed at 700 °C and 0.35 mbar during CeO_2 and BTO deposition in the case of BTO-based multilayers, and 720 °C and 10^{-2} mbar during CeO_2 and STO deposition in the case of STO-based multilayers. LSMO was deposited at 720 °C, in 0.35 mbar of oxygen. The same conditions routinely result in high quality epitaxial films on (001) STO substrates [12]. Immediately after LSMO deposition, 700 mbar of oxygen was introduced in the chamber and the films were cooled to ambient temperature at 20 °C min^{-1}. The typical layer thicknesses were 25–50 nm, 30 nm, 50 nm, 10 nm and 70 nm for LSMO, BTO, STO, CeO_2 and YSZ, respectively. The growth temperature and the partial oxygen pressure during the deposition and the thickness of each layer were optimized in order to improve the crystallinity and to maximize T_C.

3. Experimental results

We found that both the BTO-based and STO-based multilayers are highly textured, and (001) oriented (figure 1(a)). YSZ grows in *cube on cube* mode on Si, as proved by the φ-scans (figure 1(b)) that demonstrate the perfect alignment of the $(113)_{YSZ}$ and $(113)_{Si}$. Typically, the (002) YSZ rocking curve has 0.8° full width at half-maximum (FWHM). The YSZ films exhibit a very smooth surface with a root mean square (RMS) roughness of 0.4 nm over 10×10 μm^2 surface areas as revealed by atomic force microscopy (AFM). Because of its small thickness, the CeO_2 layer is not detected using x-ray diffraction. However, it is known that CeO_2 grows in *cube on cube* mode on YSZ (see, e.g., [9–11]), and this is also indirectly indicated by the crystallographic orientation of the subsequent layers in our study. When missing, no epitaxial growth ever takes place on top of YSZ. We now itemize the description of the other layers in the structures. (i) BTO-based multilayers. The φ-scans (figure 1(b)) of the (2 2 32) BTO reveal a domain structure, with a main component oriented according to the relation $(110)_{BTO} \parallel (110)_{Si}$. The φ-scans of the (303) LSMO confirm that, due to the crystal matching conditions, LSMO grows in *diagonal on cube* mode on BTO. However, the domain structure of BTO (revealed by extra peaks in the (2 2 32) BTO φ-scan) results in a two-domain structure of LSMO. In order to determine the strain in the structure, we performed x-ray reciprocal space mappings (RSM) in the region of the symmetrical (00l) and of the asymmetrical (113) YSZ, (1 1 21) BTO and (103) LSMO diffraction peaks (figure 1(c)). As a result, we found that the LSMO top layer is under in-plane compression (with 0.3838(4) nm and 0.3864(4) nm lattice spacing for 50 nm and 25 nm thick film, respectively). The LSMO out-of-plane axis is slightly elongated (0.18% and 0.52% for 50 nm and 25 nm thick LSMO, respectively). (ii) STO-based multilayers. In this case, the φ-scans in figure 1(b) demonstrate one-domain growth of both STO and LSMO. Due to the crystal matching conditions, STO grows in *diagonal on cube* mode on CeO_2, while LSMO grows in *cube on cube* mode on STO. The LSMO layer is fully in-plane strained on STO (with in-plane axes 0.3906(2) nm) for both LSMO thicknesses considered (50 and 32 nm). The out-of-plane axis is compressed by about 0.72% and 0.65% for 50 nm and for 32 nm thick LSMO, respectively. The low temperature resistivity values at 10 K, called the residual resistivity ρ_0, give an additional quantitative evaluation of film quality. They confirmed the x-ray data since ρ_0 was 3 mΩ cm for the BTO-based case, whereas ρ_0 for the STO-based case (0.7 mΩ cm) was close to ρ_0 measured for the reference sample (0.2 mΩ cm).

Cross-section transmission electron microscopy (TEM) analyses were performed on both BTO-based and on STO-based multilayers. The YSZ/Si interface is shown in figure 2(a). It is characterized by an amorphous, 2–3 nm thick

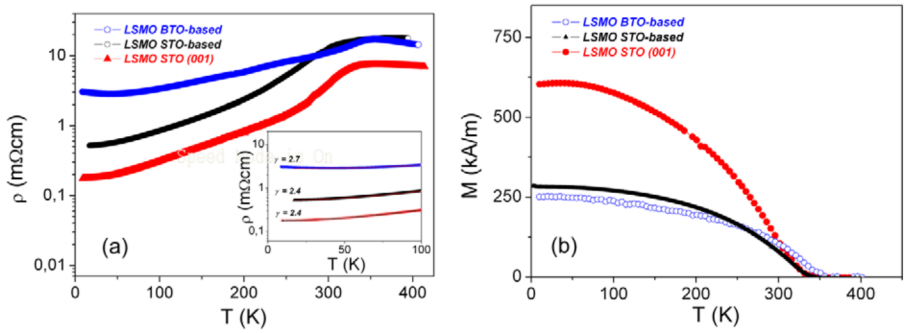

Figure 3. Resistivity versus temperature (a) and magnetization versus temperature (b) of STO-based (black line) and BTO-based (blue line) LSMO (50 nm thick) samples compared with LSMO grown on STO single-crystal substrate, (001) oriented (red line). The inset shows the $\rho(T) \sim T^{\gamma}$ behaviours in the low temperature region.

layer. In principle, it may be either residual native silicon oxide, or a layer that is formed during deposition. Indeed, during the multilayer growth some oxygen may diffuse toward the substrate surface and react with Si. This assumption may explain why, despite the amorphous layer, YSZ is highly textured and epitaxial on Si [5]. The LSMO/BTO and LSMO/STO interfaces are shown in figures 2(b) and (c). In both cases the LSMO layer is highly textured. However, the BTO-based sample presents more defects, in the form of vertical grain boundary planes running across the whole thickness of LSMO, and originated at steps at the BTO/LSMO interface. This is due to the huge vertical spacing of the BTO unit cell (3.28 nm). In contrast, the LSMO/STO interface shows a much better network continuity and good crystalline quality.

We determined the resistance versus temperature curve $\rho(T)$ using a four-point contact geometry (figure 3(a)) and the magnetization versus temperature $M(T)$ of some BTO- and STO-based samples, and of the reference sample (deposited on STO single crystal) using a superconducting quantum interference device (SQUID) magnetometer (figure 3(b)). As shown in figure 3(b), T_C is highest for the BTO-based sample (360 K), while for the STO-based sample it is about 350 K, that is still slightly higher than that for the reference LSMO film (345 K). Both multilayers show a low saturation magnetization (1.4 μ_B/Mn for the BTO-based case and 1.5 μ_B/Mn for the STO-based case at 10 K), to be compared with 3.2 μ_B/Mn for LSMO films with thickness in the range (30–50 nm), possibly due to non-magnetic regions distributed in the volume of the LSMO.

Figures 4(a) and (b) show the $M(H, T)$ loops of 50 nm thick LSMO films with the magnetic field applied along the two in-plane directions in the cases of the BTO- and STO-based LSMO, respectively. Except at 10 K for the BTO-based LSMO, no clear in-plane magnetic anisotropy is found, like for typical LSMO films on (001) STO films.

4. Analysis and discussion

When evaluating the results in terms of the perspective of application at room temperature, T_C values above ~300 K are required. Most important for our scope is the observation

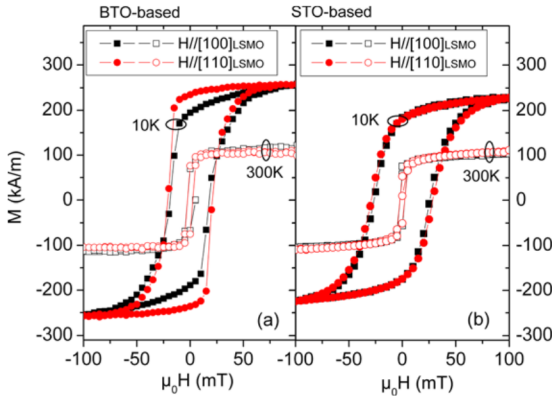

Figure 4. $M(H, T)$ loops of 50 nm thick LSMO films with the field applied along the two in-plane directions in the case of the BTO-based (a) and STO-based LSMO (b).

that the experimental differences in T_C for the two kinds of multilayers is just due to the strain. The reason is that the LSMO cell is under a compressive biaxial stress in the BTO-based case, that is known to enhance T_C [15]; while the stress is tensile in STO-based multilayers and in LSMO films. When evaluating the strain effect, we found quantitative agreement with the model of Millis *et al* [16], who expressed the Curie temperature as $T_C = T_C^0(1 - a\,\varepsilon_B - b\,\varepsilon^{*2})$. Here T_C^0 is the Curie temperature of the unstrained LSMO, $\varepsilon_B = \frac{1}{3}(\varepsilon_{[001]} + 2\varepsilon_{[100]})$ is the bulk strain and $\varepsilon^* = \frac{1}{2}(\varepsilon_{[001]} - \varepsilon_{[100]})$ is the Jahn–Teller strain, related to the distortion of the Mn octahedra under a biaxial stress. In our case, $\varepsilon_{[001]} = \frac{c_{[001]} - c_0}{c_0}$ and $\varepsilon_{[100]} = \frac{c_{[100]} - c_0}{c_0}$ are the experimental strains along the [001] (out-of-plane) and [100] (in-plane) directions, where $c_0 = 0.3873$ nm is the pseudocubic, unstrained lattice parameter of bulk LSMO. By fitting the T_C for BTO-based and STO-based samples of two different LSMO thicknesses, i.e. 30 and 50 nm, we found $T_C^0 = 345$ K, $a = 5$ and $b = 310$, which are in reasonable agreement with the literature, especially considering that the reported values of a and b are spread over quite a wide range [15, 17]. In spite of the lower T_C, the STO-based samples show smaller values of ρ_0 than the one measured in the BTO-based case. In our view, this is connected to a higher degree of disorder in BTO-based multilayers. The structural disorder is

demonstrated by the x-ray diffraction (broader rocking curves) and by TEM. The low temperature behaviour of the resistivity is a further probe of the electronic disorder in LSMO [18]. In the case of STO-based samples, the $\rho(T)$ plots follow the same dependence of resistivity on temperature as LSMO films, even if the resistivity is slightly higher (figure 3(a)), possibly due to a poorer connectivity between grains (i.e., lower degree of percolation). In the low temperature region, the plots follow the law $\rho(T) \sim T^{\gamma}$ (inset of figure 3(a)), with $\gamma \approx 2.4$. The case of BTO-based samples is a bit different. Beside the higher resistivity, a minimum of $\rho(T)$ occurs at about 50 K (figure 3(a)). Above the minimum, the exponent in the power law is $\gamma \approx 2.7$. We recall that highly ordered films show $\gamma \approx 2.5$, and that γ increases with disorder [18].

In conclusion, epitaxial LSMO films have been grown by PLD on (001) Si by resorting to a complex sequence of buffers. We compared the structural, morphological, magnetic and residual resistivity of $La_{0.7}Sr_{0.3}MnO_3/Bi_4Ti_3O_{12}/CeO_2/YSZ/Si$ (BTO-based), and $La_{0.7}Sr_{0.3}MnO_3/SrTiO_3/CeO_2/YSZ/Si$ (STO-based) multilayers. BTO-based samples are less ordered, in terms of both structure and low temperature electric transport properties. In spite of that, they show a higher T_C, due to more favourable strain conditions. STO-based multilayers, on the other hand, show a better structure and surface morphology, and a lower residual resistivity. Such properties demonstrate that, after our careful work of optimization of the growth conditions, the realization of high structural quality LSMO films is possible on (001) Si substrates using a standard PLD system, instead of high vacuum dedicated deposition systems. This is crucial for the technological development of innovative applications such as in bolometers or spintronic devices operating at room temperature.

References

[1] Ramesh R and Schlom D G (ed) 2008 *MRS Bull.* **33** (issue 11)
Bibes M and Barthelemy A 2007 *IEEE Trans. Electron Devices* **54** 1003

[2] Bergenti I, Dediu V, Arisi E, Cavallini M, Biscarini F, Taliani C, de Jong M P, Dennis C L, Gregg J F, Solzi M and Natali M 2007 *J. Magn. Magn. Mater.* **312** 453

[3] Haghiri-Gosnet A-M and Renard J-P 2003 *J. Phys. D: Appl. Phys.* **36** R127–50

[4] Scotti di Uccio U, Davidson B, Di Capua R, Miletto Granozio F, Pepe G, Perna P, Ruotolo A and Salluzzo M 2006 *J. Alloys Compounds* **423** 228
Mercone S, Méchin L, Perroni C A, Routoure J M, Scotti di Uccio U, Maritato L and Cataudella V 2007 *Prog. Solid State Chem.* **35** 387

[5] Wang S J and Ong C K 2002 *Appl. Phys. Lett.* **80** 2541

[6] Méchin L, Villégier J C, Rolland G and Laugier F 1996 *Physica* C **269** 124
Méchin L, Huot G and Bloyet D 2004 *Appl. Phys. Lett.* **85** 3154

[7] McKee R A, Walker F J and Chisholm M F 1998 *Phys. Rev. Lett.* **81** 3014
Mi S B, Jia C L, Vaithyanathan V, Houben L, Schubert J, Schlom D G and Urban K 2008 *Appl. Phys. Lett.* **93** 101913

[8] Goh W C, Yao K and Ong C K 2005 *J. Appl. Phys.* **97** 073905

[9] Fontcuberta J, Bibes M, Martínez B, Trtik V, Ferrater C, Sánchez F and Varela M 1999 *J. Appl. Phys.* **85** 4800

[10] Kim J H, Khartsev S I and Grishin A M 2003 *Appl. Phys. Lett.* **82** 4295

[11] Kim J H, Grishin A M and Radamson H H 2006 *J. Appl. Phys.* **99** 014903

[12] Yang F, Méchin L, Routoure J M, Guillet B and Chakalov R A 2006 *J. Appl. Phys.* **99** 024903
Méchin L, Routoure J M, Guillet B, Yang F, Flament S, Robbes D and Chakalov R A 2005 *Appl. Phys. Lett.* **87** 204103

[13] Ruotolo A, Oropallo A, Miletto Granozio F, Pepe G P, Perna P and Scotti di Uccio U 2006 *Appl. Phys. Lett.* **88** 252504
Ruotolo A, Oropallo A, Miletto Granozio F, Pepe G P, Perna P, Scotti di Uccio U and Pullini D 2007 *Appl. Phys. Lett.* **91** 132502

[14] Kim J H and Grishin A M 2005 *Appl. Phys. Lett.* **87** 033502
Méchin L, Villégier J C and Bloyet D 1997 *J. Appl. Phys.* **81** 7039

[15] Tsui F, Smoak M C, Nath T K and Eom C B 2000 *Appl. Phys. Lett.* **76** 2421

[16] Millis A J, Darling T and Migliori A 1998 *J. Appl. Phys.* **83** 1588

[17] Thiele C, Dorr K, Bilani O, Rodel J and Schultz L 2007 *Phys. Rev.* B **75** 054408

[18] Mercone S, Perroni C A, Cataudella V, Adamo C, Angeloni M, Aruta C, De Filippis G, Miletto F, Oropallo A, Perna P, Petrov A Y, Scotti di Uccio U and Maritato L 2005 *Phys. Rev.* B **71** 064415
Mercone S, Perroni C A, Cataudella V, De Filippis G, Adamo C, Angeloni M, Aruta C, Miletto Granozio F, Oropallo A, Perna P, Petrov A Y, Scotti di Uccio U, Balestrino G and Maritato L 2005 *J. Supercond.* **18** 719